IET Renewable Power Generation

Research Article

IET Journals
The Institution of Engineering and Technology

Virtual inertia provision through data centre and electric vehicle for ancillary services support in microgrid

ISSN 1752-1416
Received on 27th February 2020
Revised 12th October 2020
Accepted on 20th November 2020
E-First on 16th February 2021
doi: 10.1049/iet-rpg.2020.0217
www.ietdl.org

Neethu Elizabeth Michael[1] ✉, *Shazia Hasan*[1], *Sukumar Mishra*[2]

[1]*Department of Electrical and Electronics Engineering, Birla Institute of Technology & Science Pilani, Dubai, Campus, Dubai, United Arab Emirates*

[2]*Department of Electrical Engineering, Indian Institute of Technology Delhi, New Delhi, India*

✉ *E-mail: neethubitspilanidubai@gmail.com*

Abstract: The proposal focuses on the role of data centres (DCs) and electric vehicle (EV) energy storage systems (ESSs) for frequency regulation and it provides a new opportunity for different resources to participate in the power sector. Frequency fluctuations are introduced with the emergence of inverter-dominated renewable energy sources (RESs) as it does not provide rotational inertia to the grid, such as synchronous generators. In this study, the virtual synchronous generator (VSG) controlled inverter compensates for the lack of inertia. Particularly, this research work analyses the involvement of DC and EV batteries as ESSs in designing an integrated technical virtual power plant (VPP) to support frequency variations using the VSG concept. Microgrid (MG) simulations are performed in MATLAB/ Simulink platform. Case studies are carried out to validate the grid export and grid import performance of the model by using variations in the load and the solar irradiance of the MG. It is verified that bidirectional power flow takes place between the proposed VPP components and the grid that enables the grid with high penetration of RESs. The work provides a conceptual framework for future contributions towards the smarter usage of assets such as ESS and a greener future.

1 Introduction

1.1 Literature review

The environmental issues we are experiencing today necessitate prospective long-term actions and hence renewable energy technology is inextricably linked to sustainable development [1]. The new microgrid (MG) concept is highly impressive as a potential solution and is typically associated with power electronic inverters with the load and utility grid [2]. Therefore, the large penetration of renewable energy resources (RESs) enables the MG to migrate from a controlled rotational generator system to an inverter-dominated system [3]. Besides the diverse advantages of MGs, it faces various challenges such as insufficient frequency response due to the disparities in the load/generation equilibrium, control issues, and even security problems.

Frequency response which is provided by governor action and load occurs within the first few seconds after a frequency disturbance to maintain stability. If the inertial response lowers, it results in an excessive rate of change of frequency (ROCOF) and a low-frequency nadir (minimum frequency point) in a very short period (<10 s) as depicted in Fig. 1. This kind of circumstance can lead to frequency relay's tripping [4], in the worst scenario, to cascaded outages. One of the blackouts have occurred on 1 November 2014, Bangladesh Power System (BPS) had a nationwide blackout in a whole day [5]. It was observed that a high-voltage direct current station had a collapse and the spinning reserve did not respond. It was recommended that the BPS system should maintain the critical operating inertial reserve to be >9 s, thus improving the under-frequency protection scheme by considering the ROCOF. Several cases are reported and most of the causes of the blackout are associated with transmission system operation, control, and protection [6].

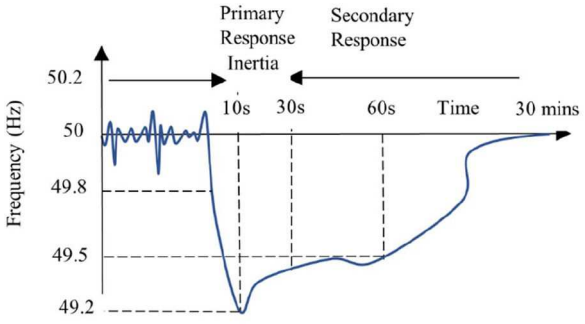

Fig. 1 *Time frame for frequency response [7]*

Several studies have focused on the regulation of MG frequencies and have used alternate methodologies for frequency control [8]. Researchers address photovoltaic (PV)-based MG's [9] and describe different topologies of PV inverters [10]. However, the authors have not used any ESS as a backup for the MG. The researchers analysed the frequency regulation in a wind–diesel-powered MG using flywheels and fuel cells. In [11], the authors suggested different control algorithms that utilised wind power for regulating the frequency of islanded MG. However, owing to the seasonal and unreliable nature of wind, this concept was inefficient to regulate the frequency of MG's. Hence, RESs such as PV and wind alone cannot be used for the frequency regulation of the MG. Even though wind turbines have rotational mass, PV systems are not associated with any and cannot provide inertia to the system. Several authors have used the ESS for the frequency regulation of MG [12] but, they have not considered inertia to regulate frequency. Thus, as the world is progressing towards the era of renewable energy sources (RESs), the research on presenting inertia virtually to the system has gained momentum.

Beck and Hesse [13] first initiated the idea of virtual inertia (VI) implementation using power electronic converters to emulate inertia. The literature has since established many other VI topologies [4, 13] and its main parts are RESs, ESSs, control algorithms, and power electronics. Different types of ESSs, their control methods, and operational characteristics are reviewed by Arani *et al.* [14]. However, in the context of the present ESS technology progress, more efficient control strategies are expected for ESS design to support MG operation. Most recently, Aly *et al.* [15] have explained the role of flywheel ESSs using Homer software in MG design. Liu *et al*. [16] have described that the PV–virtual synchronous generator (VSG) control strategy can be used

to decay disturbances easily thus enhancing the transient stability of the power system with high penetration of PV's. Though there are various studies on VSG, simulations were carried out in MGs, and the capacity of ESS in PV was not evaluated in detail. Li *et al*. [17] have discussed VSG-based Synchronous Compensator [STATCOM] for wind farm voltage regulation. However, it takes a much longer time to reach a steady-state after input load variation because STATCOM has little frequency regulation capability. Ma *et al*. [18] have illustrated a comprehensive VSG control strategy for the system of full converter wind turbine, focusing on the energy balance and showed better frequency response. The authors have also considered research studies comparing VSG and droop control and have discussed the advantages of the VSG over the droop method. It has been observed that the VSG mechanism has better feedback in the stabilisation of an MG [19]. Wang *et al*. [20] have examined a VSG-based adaptive PV-droop control for frequency and active power regulation.

The authors have addressed that electric vehicles (EVs) can provide redundancy, reliability, and stability where RES is used [21]. The use of rechargeable batteries in EVs is the most cost-effective as the utilities barely need any maintenance or installation cost. However, some researchers have addressed the issue of aging of state of charge (SoC) of batteries, which should be investigated for better primary frequency regulation. In recent studies, Dhingra and Singh [22] have explored the role of the EV charging station (CS) to support MG frequency. It has been observed that the required power is delivered or absorbed by the EV CS to support the frequency of the system.

However, it is also expected that by introducing other asset owners, the exchange of energy through inverters between the available ESS and the power system can be reduced. One advantage of using these services is that they are independent of variable energy input variations. In this context, the coordinated control of ESSs of EV and DC [23] can be utilised for power system frequency regulation, especially for MGs. The authors have demonstrated the use of data centres (DCs) as a virtual power plant (VPP) in demand response [24]. Awasthi *et al*. [25] detailed how the DC can operate as a VPP with the integration of renewable energy and other available resources. Though it helped to understand the minimisation of generation cost, it did not consider the intermittent nature of RES [25]. It has been observed that several authors emphasised the potential of using large-scale DCs to provide frequency regulation and participation in the power market. However, no one has explored the application of VSG in DCs for frequency regulation [26, 27].

1.2 Motivation

Frequency fluctuations due to the dynamic load profile of RES results in the instability of MG. Considering the reliability of the MGs against partial/full blackouts and the future goal to accommodate a high penetration of RES, this paper proposes the concept of VI. As stated in Section 1.1, the concept of VI has been defined throughout the literature [3, 4, 28]. Besides self-reliant battery energy storage systems(ESS), the role of EV batteries as ESS is increasingly being looked at to perform ground-to-vehicle (G2V) and vehicle-to-ground (V2G) operations with frequency support [29]. In the proposed work, we discuss the participation of DCs in the power market [19, 25, 27, 30]. Several DC operators have also proposed their power generation capacity as secondary reserves for the ancillary services industry. With the appropriate control algorithms and capabilities of modern uninterrupted power supply (UPS) technology and batteries, the use of battery power can be controlled smoothly [31].

Depending on the literature reviews, there are no studies that utilise the VSG topology for the effective use of EV and DC ESS to form a VPP in the same geological area for compensating frequency fluctuations in a MG. The freshness of this concept lies in the following subsection.

1.3 Novelty

The paper's uniqueness lies in the following factors. First and foremost, EV and DC UPS ESS are integrated to form a technical VPP (TVPP) for frequency regulation using the concept of VSG. Here we call it TVPP since it does not consider the operational cost details. As per the authors' knowledge, no work is being researched to regulate frequency involving different resources in the same geographical area. In the second place, each battery source is controlled and managed with independent bidirectional converters and energy management systems (EMSs). Therefore, considering the future large-scale penetration of RES, EVs and even DCs, the proposed approach would be a viable solution for maintaining the frequency of the MG.

1.4 Contribution and organisation

The contributions of this paper are as follows:

- In this paper, EV ESS and DC ESS are integrated to form a VPP and bidirectional power flow between VPP and MG is controlled through the VSG concept.
- Different case studies of load unbalance, the dynamic nature of solar irradiation, availability of EV, and temperature variations are considered, and then frequency support is validated through the VSG concept.
- The VPP control method includes an independent set of rules for regulating the SoC of batteries and helps to identify the working mode of battery, i.e. grid import/charge mode or grid export/ regulating mode.
- It is an added advantage that different resources can be independently managed with the same concept.

The paper is organised as follows, Section 2 details the EV and DC integrated VPP. Section 3 describes the control method and power system modeling using VSG, Section 4 explains the simulation and results, Section 5 includes the conclusion, and Section 6 contains references.

2 EV and DC-integrated VPP

The paper's concept is to use the VPP concept for providing frequency stability. Both MG and VPP are attractive to provide integration of distributed energy resources in the electricity network. The VPP is introduced to make MG integration smooth without compromising grid stability and reliability [32, 33]. The essence of a VPP is an EMS that coordinates the current flow from the generators, loads, and storages. The interactions are bidirectional, so that information is not only available to the VPP about each unit's current status but can also send the signals for participant's controls.

The concept of VPP with EV is significant in the electricity market due to the high penetration of EV's in the market. Researchers have suggested the strategy of using the available energy resources for a TVPP. In [34], the authors have mentioned PV units, microturbines, and EV as TVPP for the optimal solution. TVPP can maximise its profit in the day-ahead market by using an energy scheduling framework. The demand response capability of TVPP also helps in maximising its profit. An energy management-based strategy helps in the economic planning of VPP and can address the electrical constraint of the power system. Such studies have the key objective to devise a system for the participation of the VPP controller in energy markets under varying system conditions and uncertainties while facilitating the integration of the VPP in power systems by supporting ancillary services [35]. Researchers have also worked on the scheduling strategy of VPP considering sources such as EV, wind power plants, and PV to guarantee the maximum overall expected profit achievement. Moreover, the VPP model considering the degradation cost of the ESS is also under research for maximising the expected profits of VPP [36].

It is well known that batteries are the most important components of EVs and DCs. EV batteries which are one of the power exchanging components of VPP are charged at regular intervals from a CS in the power grid for commercial utilisation. In the case of DCs, the underutilised resources such as UPS batteries or supplementary batteries appending to the existing plants can also

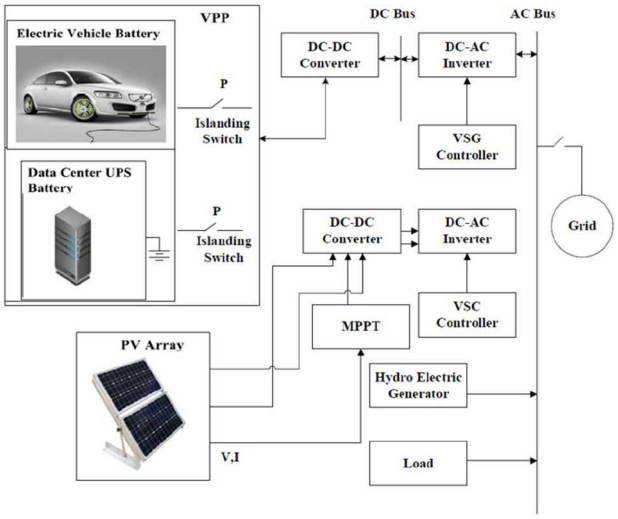

Fig. 2 *Single line diagram of the VPP and MG*

take an interest in the power industry by embedding effective control algorithms appropriately. Additional batteries can be installed to existing UPS systems, to reduce the initial capital cost and they can be used in ancillary services. This concept can be realised as almost all DCs have UPS systems as a resource backup and hence it represents a significant investment in DCs [37]. Eaton has developed modern UPS, called 'Energy-aware UPS' (Eaton's Energy Aware 93PM and 9395P UPS) with many supporting features that can contribute actively to the grid by using the VI concept.

Hence the integrated EV and DC VPP concept used here presents an autonomous power source during unforeseen responses in the power system. Components of VPP are isolated from the dc bus using the islanding switch. Fig. 2 details the single line diagram of the model considered for this study. MG collaboration with integrated VPP between EV's and DC enhances the process for both parties, (i) the VPP gains grid power to charge batteries when increased power is available on the ac grid and (ii) the VPP can respond to the grid during a significant load event or address PV fluctuations by discharging energy from the batteries. This research permits optimal use of the capacity of VPP elements to provide frequency regulation. This encourages small units to provide ancillary services and lowers the risk of power quality through power-sharing.

As the number of non-rotating energy sources such as PVs increases, controlling the available battery power in EVs and DCs helps improve feeder operation and reduces the need for added grid infrastructure [38]. Thus, both EV and DC exchange active power to dc bus based on the power availability on the grid. The EV and DC battery can operate in G2V/grid import as well as V2G/grid export mode of operation and can contribute to frequency regulation and power exchange. So, at some point, the batteries can inject power to the MG and at the same time, it behaves as a load depending on the conditions of battery charge and power availability at the MG side.

3 Control method and power system modeling using VSG

3.1 Proposed methodology

In the proposed work, a MG consisting of a PV array and hydro-electric generator is used. A power inverter with VSG powered topology links the proposed MG to the dc bus, transfers active power to and from the system, and maintains a constant dc voltage using the VSG controller. EV batteries and DC UPS are connected to the dc bus via a bi-directional converter and EMS. The various components of the model are detailed in the below sub-sections.

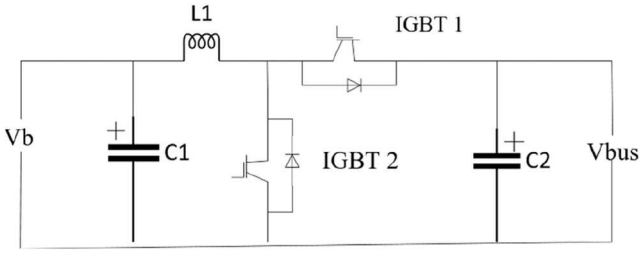

Fig. 3 *Design of the buck–boost bi-directional converter*

3.2 Bi-directional dc–dc converter

The VPP is connected to the MG through a bi-directional dc–dc converter. In this research, a non-isolated type bi-directional converter is used since it has less weight, low loss, less price, and transformerless configuration. To prevent the battery from overcharging and over-discharging, the charging method should be adequately selected. Bi-directional dc–dc converter for battery uses constant voltage (CV) and constant current (CC) control strategies to achieve the best performance during regulation and charge mode of operation [39]. Buck and boost pulses are generated through two control loops. In CV mode, the battery voltage is compared with the reference voltage and it passes through a controller. In CC mode, the battery current is compared, and if it is positive, the battery is charging, and if it is negative, then it goes to the discharge mode of operation. Two proportional–integral controllers are implemented to achieve the desired reference signal. Buck and boost pulses are given to insulated-gate bipolar transistors (IGBTs) based on the control input. Thus, bi-directional dc–dc converters are used here to step up or step down the voltage thus enabling the charging and discharging process as well as regulating dc bus voltage. Fig. 3 shows the design of the buck/boost bi-directional converter.

IGBTs are used as switching devices due to their high-switching frequency and low-switching losses. The IGBTs 1 and 2 are complementary and it guarantees that the current of the inductor is continuous throughout the process. When IGBT1 operates, the inductor L stores energy and the circuit works in boost mode of operation. When IGBT2 functions, the circuit goes back to the buck mode of operation. The design requirements of bidirectional buck–boost dc–dc converter incorporating with ESSs are described by the (1)–(3). The values of L, C_1, and C_2 give the critical values of inductances and capacitance to maintain continuous inductor current and continuous capacitor voltage. The inductor and capacitance values are chosen higher than the designed values as defined in the following equations to maintain MG stability. V_b represents the battery side voltage and V_{bus} represents the dc bus side voltage

$$L = \frac{V_b}{0.6(P_o/V_b)f_s}\left(1 - \frac{V_b}{V_{bus}}\right) \tag{1}$$

$$C_1 = \frac{D_2 V_b(1 - D_2)}{8 f_s^2 L \Delta V_c} \tag{2}$$

$$C_2 = \frac{(P_o/V_{bus})\ D_1}{f_s L \Delta V_c} \tag{3}$$

D_1 and D_2 are the duty cycles considered in buck and boost mode of operation, ΔV_c is the capacitor ripple voltage, f_s is the switching frequency, which is taken as 25 kHz to avoid high-frequency noise and other disturbing elements, and P_o is the output power. The dc–dc converter is tested and validated in the MATLAB/Simulink environment.

3.3 VSG enabled converter-mathematical formulation

VSG topology is employed to mimic the inertia of the synchronous generator so that the system receives the required inertia to compensate for the frequency variations. Frequency fluctuations

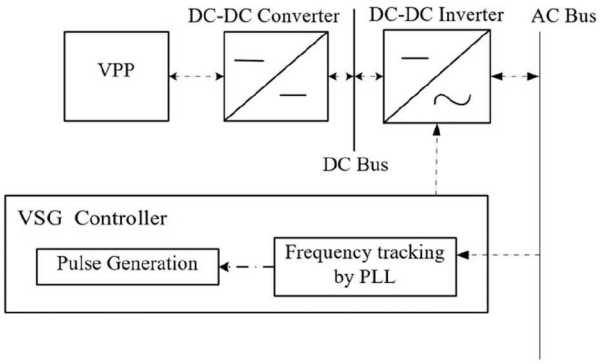

Fig. 4 *VSG mechanism and interaction of VPP with MG*

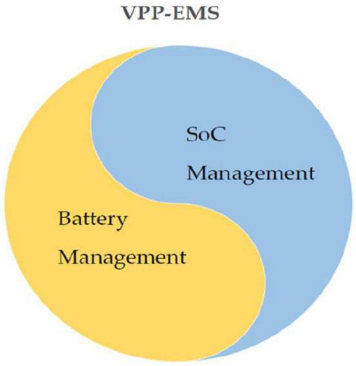

Fig. 5 *EMS-heart of VPP*

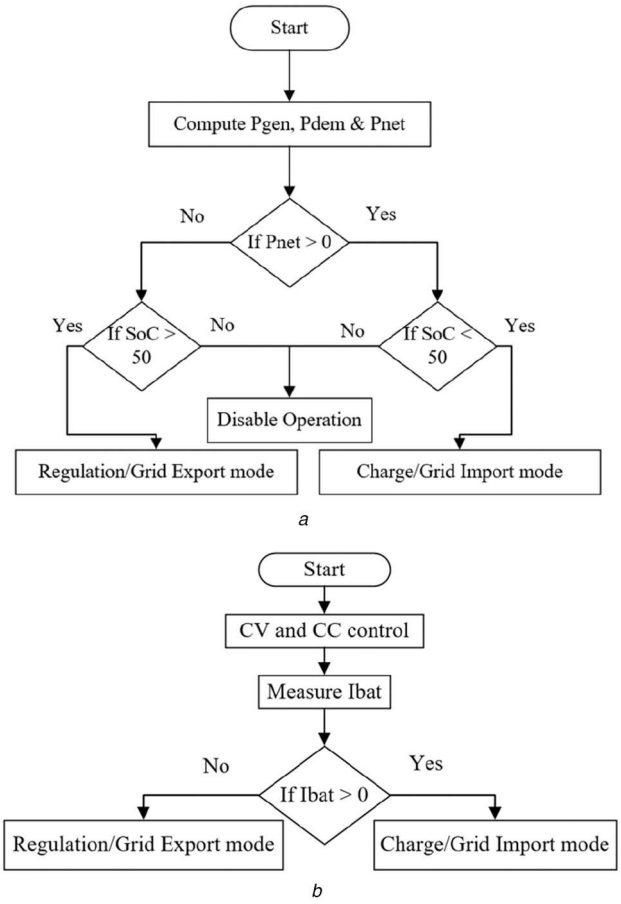

Fig. 6 *Flow chart of energy management scheme*
(a) SoC management, ***(b)*** Battery current management

result due to the unpredictable behaviour of RES and fluctuations in the load requirement irrespective of the power generation. So, this method compensates for the disturbances and makes the system more stable. Here the dc bus link voltage is kept constant and the VSG concept is accomplished by maintaining system voltage and synchronism. The reference power, P_{vsg} is generated using the following equation. Here the frequency derivative method is utilised to formulate the VSG algorithm. Equations (4)–(8) constitute the VSG mechanism

$$P_{\text{vsg}} = K_{\text{i}}\frac{\text{d}\Delta f}{\text{d}t} + K_{\text{d}}(\Delta f) \tag{4}$$

$$K_{\text{i}} = \frac{P_{\text{vsg}_{\text{nom}}}}{(\text{d}(\Delta f)/\text{d}t)\ \max} \tag{5}$$

$$K_{\text{d}} = \frac{P_{\text{vsg}_{\text{nom}}}}{(\Delta f)\ \max} \tag{6}$$

$$i_{d\text{ref}} = \frac{2}{3}\ \frac{V_d P_{\text{vsg}} - V_q \text{Q}}{V_d^2 + V_q^2} \tag{7}$$

$$i_{q\text{ref}} = \frac{2}{3}\ \frac{V_d Q - V_q P_{\text{vsg}}}{V_d^2 + V_q^2} \tag{8}$$

Here K_{i} is the inertia constant, K_{d} is the damping constant, Δf is the frequency deviation of the system. Here 60 Hz is taken as the nominal frequency. K_{i} and K_{d} determined by using (5) and (6) [40]. K_{i} makes the VSG to counteract the frequency deviations and K_{d} brings back the frequency to normal value. $P_{\text{vsg\_nom}}$ is the nominal power rating. (Δf) max is the maximum change in frequency and $(\text{d}\Delta f/\text{d}t)$ is the maximum ROCOF. The equivalent direct axis current, i_d, and quadrature axis current, i_q, to generate the reference active power and reactive power is then calculated based on (7) and (8), where P_{vsg} is the reference active power, Q is the reference reactive power, V_d is the direct axis voltage, and V_q is the quadrature axis voltage. Fig. 4 shows the VSG mechanism and interaction of VPP with the MG. The value of reference dc voltage is selected such that the modulation index is kept at 1 pu voltage. The value of V_{dc} is calculated by

$$m = \frac{V_{\text{L}}\sqrt{2/3}}{V_{\text{dc}}/2} \tag{9}$$

where m is the modulation index, V_{L} is the line voltage, and V_{dc} is the dc-link voltage.

The phase-locked loop measures the MG frequency and the ROCOF using the MG voltage V_{abc}. The control algorithm then calculates P_{vsg} using (4) to generate the reference current i_d for the controller. The dc voltage regulator and decoupled d/q controller are used to generate the required gate pulses for charging and discharging processes. Thus, it exchanges active power between VPP and MG. The controller also helps to protect the power converter against overload and external failures.

3.4 VPP–energy management system

Fig. 5 shows the EMS operation of VPP. As shown EMS has two controllers, one is for battery management and the other is for SoC management. These two controllers operate together to determine the operating mode and thus saves battery life.

Here SoC and battery current data are used for scheduling the ESS available with EVs and DC to operate it as VPP. An SoC module, as well as a battery current controller associated with the dc–dc converter, accounts for the generation of pulses for different modes of operation.

The flowchart representation in Figs. 6*a* and *b* shows the actions performed depending on the conditions provided. The system evaluates the generated power by PV array $P_{\text{PV\_Gen}}$, generated power by a hydro-electric generator $P_{\text{Hydro\_Gen}}$, the total load P_{Load}, and the net power P_{net} available in the grid as per the below equation

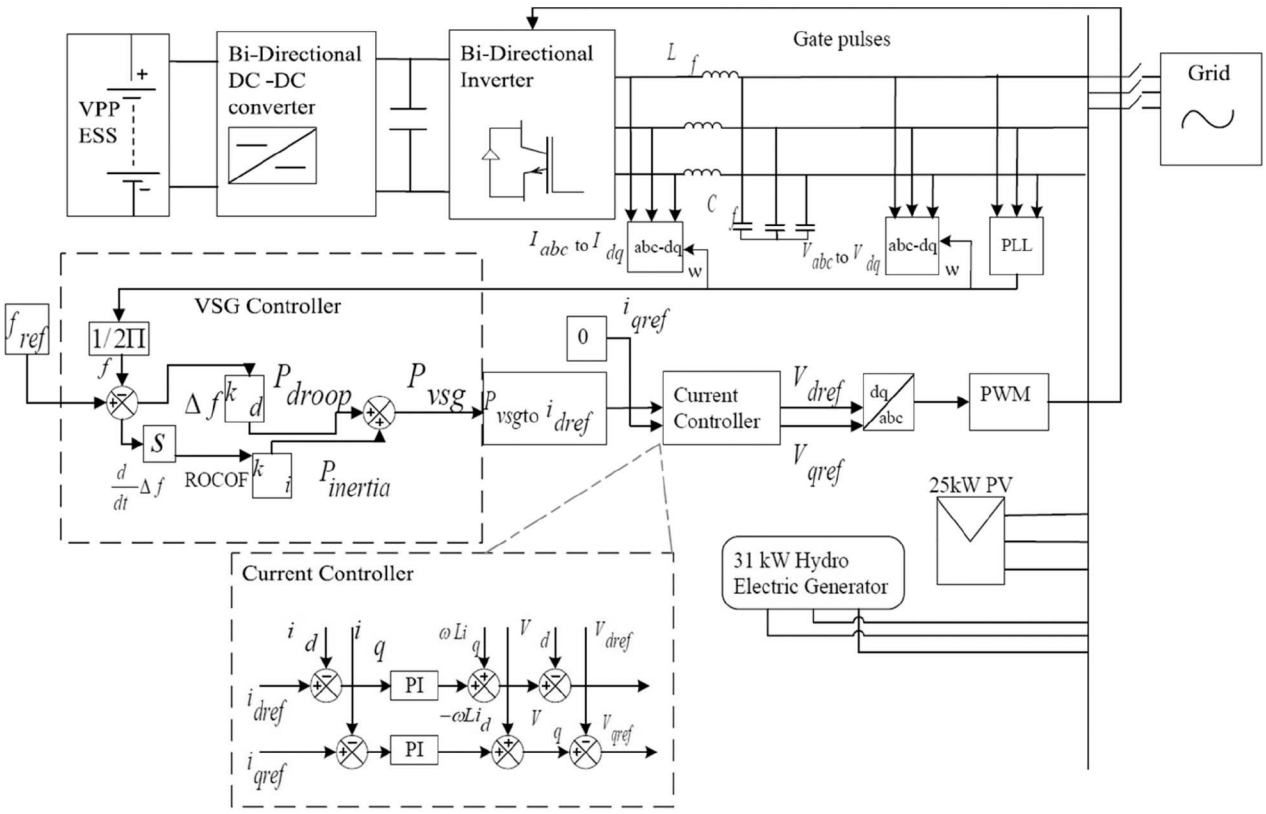

Fig. 7 *Control diagram*

Table 1 Parameter values of power system model and components

Parameters	Values
power system nominal voltage	208 V
nominal frequency	60 Hz
bi-directional DC/DC buck–boost converter, dc-link voltage	340 V
dc-link capacitors	4400 μF (Electrolytic Type)
modulation index, m	1
inductance, L	9 mH
capacitance	1200 μF (C_1 and C_2)

Table 2 Parameter values of PV model and hydro-electric generator

Parameters	Values
PV panel (330 × SunPower SPR-305E-WHT-D)	25.85 kW,208 V, three-phase PV array
VSC converter carrier frequency	33 × 60 Hz = 1.98 kHz
hydro-electric generator	39 kVA, 208 V, 31 kW
electrical power	31 kW
mechanical power, pm	47,021.1 W
stator field voltage	32.1871 V

Table 3 Parameter values of power inverter, ESS, and filter

Parameters	Values
$P_{\text{vsg\_nom}}$ of VSG controller	5600 W
K_{i}	2800
K_{d}	11,200
ESS nominal voltage	400 V
battery capacity Type	20 Ah Li-ion
power inverter switching frequency	10 kHz
LC filter	C = 10 mF, L = 3.3 μH

$$P_{\text{net}} = \left(P_{\text{PV\_Gen}} + P_{\text{Hydro\_Gen}}\right) - P_{\text{Load}} \tag{10}$$

Then it passes the gate signals to process the mode of operation depending on the conditions specified. If P_{net} available is positive and the SoC is <50% (50% is set as a trade-off percentage for safe operation and lifetime of the battery), the gate signals are transferred for charging from the MG, and the battery act as a load. Therefore, buck operation is performed using a bi-directional dc–dc converter after a positive or negative assessment of the battery current. Similarly, if the net power available, P_{net} is negative and the SoC is >50% the gate signals are transferred for discharging from the battery and it acts as a resource. Therefore, boost operation is performed using a bi-directional dc–dc converter after a positive or negative assessment of the battery current. If any mismatch of these conditions, the respective ESS gets disconnected and do not participate in the grid functioning for the safe operation of the battery and stability of the system.

4 Simulation and results

The control diagram of the proposed MG in islanded mode of operation based on the 208 V power system is shown in Fig. 7. This study has considered the battery specification of 400 V, 20 Ah as ESS. The SoC states of EV and DC batteries assumed are mentioned in the respective case studies. Thus, here, in case study I and III, two numbers of ESS with lithium-ion batteries are taken with a total capacity of 40 Ah, equivalent to 16 kWh of energy. As one of the primary energy sources in the MG, a three-phase 31 kW hydroelectric generator with a governor and excitation system is used. A 25.83 kW PV array system has been added to it, thus constituting a total power capacity of 56.85 kW.

An inductor–conductor (LC) filter is used here to minimise the harmonics during the switching process of the power inverter. Simulation parameters of PV, hydro-electric generator, VSG controlled power inverter, LC filter, and ESS are specified in Tables 1–3 [4, 20].

The PV array is connected to the grid via an ac–dc converter and a three-phase three-level voltage source converter (VSC). Maximum power point tracking (MPPT) is implemented in the boost converter using the 'incremental conductance (INC) +

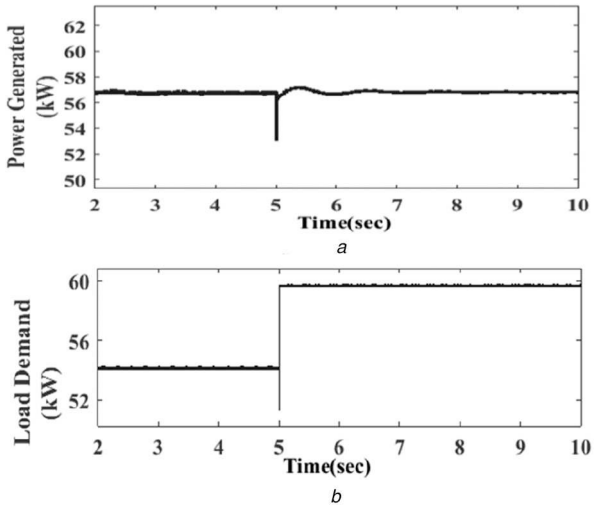

Fig. 8 *Electricity generation & load Profile during load variation*
(a) Power generated, ***(b)*** Load demand

integral regulator' technique. The INC method utilises the INC (dI/dV) of the PV array to compute the sign of the change in power to voltage (dP/dV) [41]. The INC method provides rapid MPPT even under rapidly changing irradiation conditions with higher accuracy than the perturb and observe method. The maximum power point is obtained when dP/dV = 0, where $P = V \times I$. The integral regulator minimises the error (dI/dV + I/V). Thus the switching duty cycle is optimised and the MPPT regulator starts regulating PV voltage by varying the duty cycle to extract maximum power PV array and delivers a maximum of 25.85 kW at 1000 W/m^2 sun irradiance and 25°C. PV array uses 330 SunPower modules (SPR-305E-WHT-D). The array consists of multiple strings of series-connected modules connected in parallel.

4.1 Results and discussion—case study I load variation

In the case study I, the presented system configuration is subjected to load variation while the irradiance of the PV system is kept constant at 1000 W/m^2. The load on the system is changed from the initial requirement of 54 to 59 kW at 5 s, which causes an imbalance in the system. Figs. 8*a* and *b* present the generated power (56.85 kW) and load demand. Moreover, the dc bus voltage remains constant at a reference value and shows the variation whenever there is load fluctuation as depicted in Fig. 9*a*. In this case, the EV ESS and DC ESS go through the VPP control algorithms and scrutinise which operation needs to be performed depending on their respective SoC conditions. The load imbalances are met by the EV and DC ESS. Figs. 9*b* and *c* illustrate the SoC states of EV and DC ESS, respectively. Fig. 9*d* shows the frequency of the MG with and without the VSG controller from its nominal value when the load fluctuates at 5 s.

It is observed that the EV ESS with a SoC of 10% participates in charge/grid import/G2V mode of operation until 5 s. Therefore, as shown in Fig. 10*a*, the power absorbed by EV ESS is −2750 W. Since the power demand is increased after 5 s, the EV ESS can no longer charge from the MG, and it remains inactive.

Again, DC ESS with a SoC > 50% performs the discharge/grid export mode of operation after 5 s until 7 s and starts delivering power 2050 W to balance the load demand as depicted in Fig. 10*b*.

The energy exchange is calculated over the period where the ESS exchanges power with the system. The energy exchanged by EV ESS during the charging process is −3.53 Wh and energy exchanged by DC ESS during the discharging process is 2.801 Wh. It is observed that overshoot frequencies are reduced by the proper control of the controller and power exchange through VPP.

4.2 Results and discussion—case study II irradiance variation

In this case study, Figs. 11*a* and *b* present power generated and load demand, respectively, such that the total generation on the

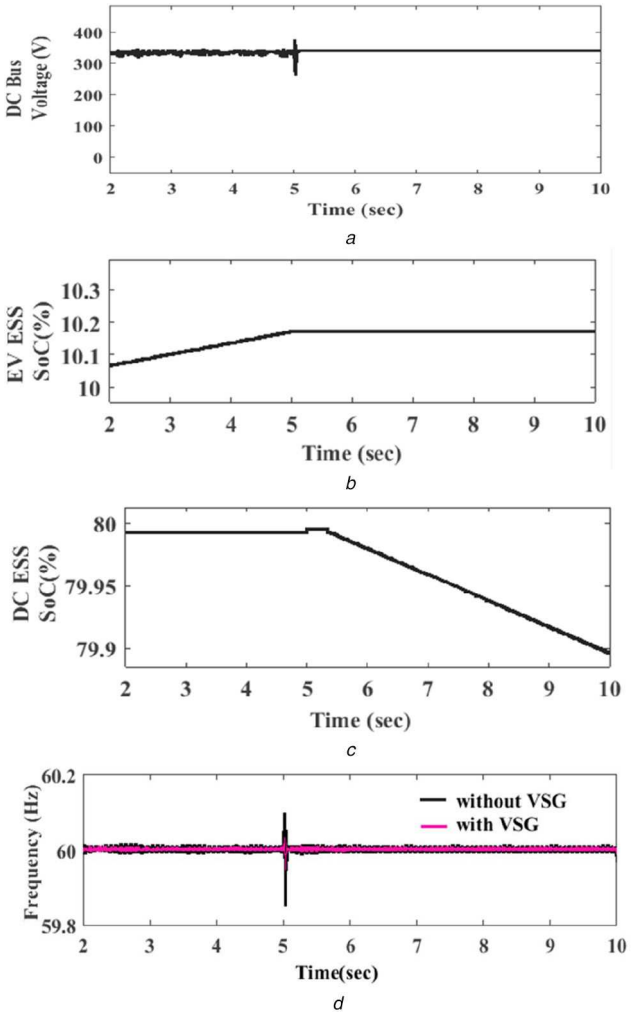

Fig. 9 *System parameters during load variation*
(a) The dc bus voltage, ***(b)*** EV ESS SoC, ***(c)*** DC ESS SoC, ***(d)*** Frequency

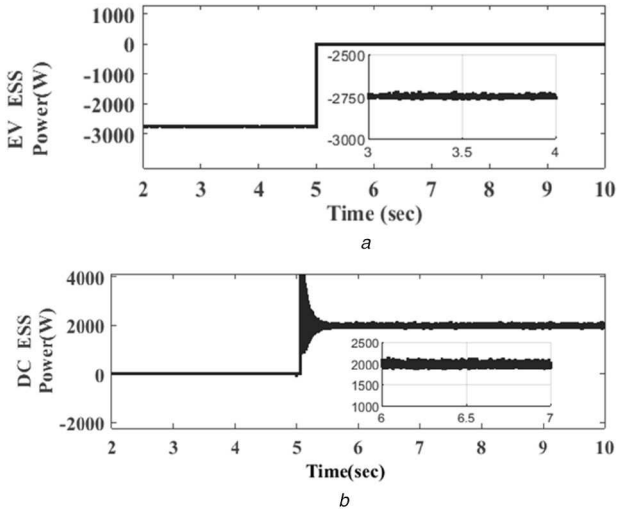

Fig. 10 *Response of ESS's during load variation*
(a) Power exchanged by EV ESS, ***(b)*** Power exchanged by DC ESS

system is 56.85 kW, load demand is 54 kW and the irradiance of the PV system is kept at 1000 W/m^2 initially. As a major consideration, the solar irradiance level is changed from the initial value of 1000 to 800 W/m^2 at 5 s as shown in Fig. 11*c* [42, 43]. Eventually, PV generation reduced from 25.85 to 20.65 kW, and the total generation is reduced to 51.65 kW, which resulted in a generation-load mismatch. Fig. 12*a* illustrates the dc bus voltage status.

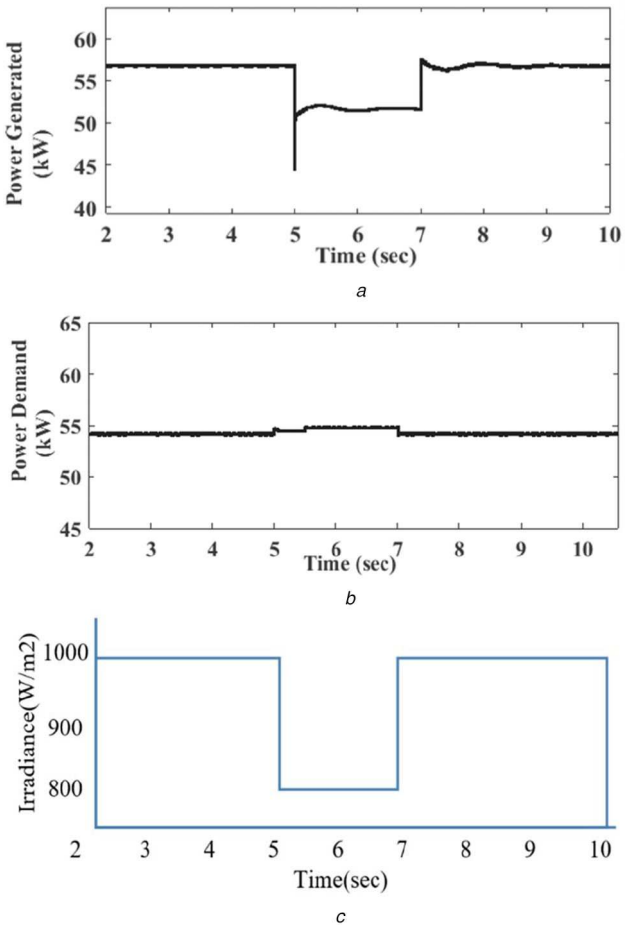

Fig. 11 *Power generated and load demand*
(a) Power generated, ***(b)*** Load demand, ***(c)*** Variable solar irradiance

Detailed forecasting methods to describe the arrival of EV, as well as the renewable energy generation, have been researched in [44, 45]. Car arrival/departure patterns for realistic storage capacity for EVs in parking lots have been discussed in [46]. However, in this paper, the dynamic behaviour of EV batteries is considered according to the forecasting performed by the crystal ball software tool. The historical data is assumed in a seasonal pattern that in CS 1, the number of EVs available is 30 at 10 a.m. of day1, 10 at 1 p.m. of day 1, and 0 vehicles at 5 p.m. of day 1. Similarly, variations in the number of EVs are assumed for four days. We categorise this prediction into three subcase studies, subcase (a) plenty of EVs; subcase (b) minimal EVs, and subcase (c) 0 EVs.

Here to analyse the perspective of arrival/departure of EVs and to exemplify the subcase (a) plenty of EVs data, one more EV battery is considered from another CS2. EV1 is assumed to be from CS1 with a SoC of 45% and EV2 from CS2 with a SoC of 90%. It is taken as that for CS1, EV1 is already available and departs at the 5 s of simulation time. EV2 of CS2 arrives at 5 s. Table 4 shows the battery status at different simulation times.

Figs. 12*a–d* show the dc bus voltage, SoC status of DC, EV1, EV2, and DC ESS. The dc bus voltage and frequency have reached a steady-state after the transient period. Moreover, Fig. 12*e* shows the frequency deviation from its nominal value when the load fluctuates at 5 s. It is observed that the power requirement is met by the EV and DC ESS.

Hence shown in Fig. 13*a*, EV1 ESS with a SoC of 45% absorbs the power of −2550 W until 5 s and performs G2V operation until 5 s. Simultaneously, DC ESS remains inactive as SoC is >50%. The energy exchanged by EV1 ESS during the charging process is −3.333 Wh. EV1 ESS departs after 5 s. Meanwhile, from 5 s, DC ESS and EV2 ESS discharge to the MG thereby performing the discharge/grid export mode of operation. Therefore, as depicted in Figs. 13*b* and *c*, EV2 ESS starts delivering power 1075 W and DC ESS starts delivering power 975 W to balance the system. During

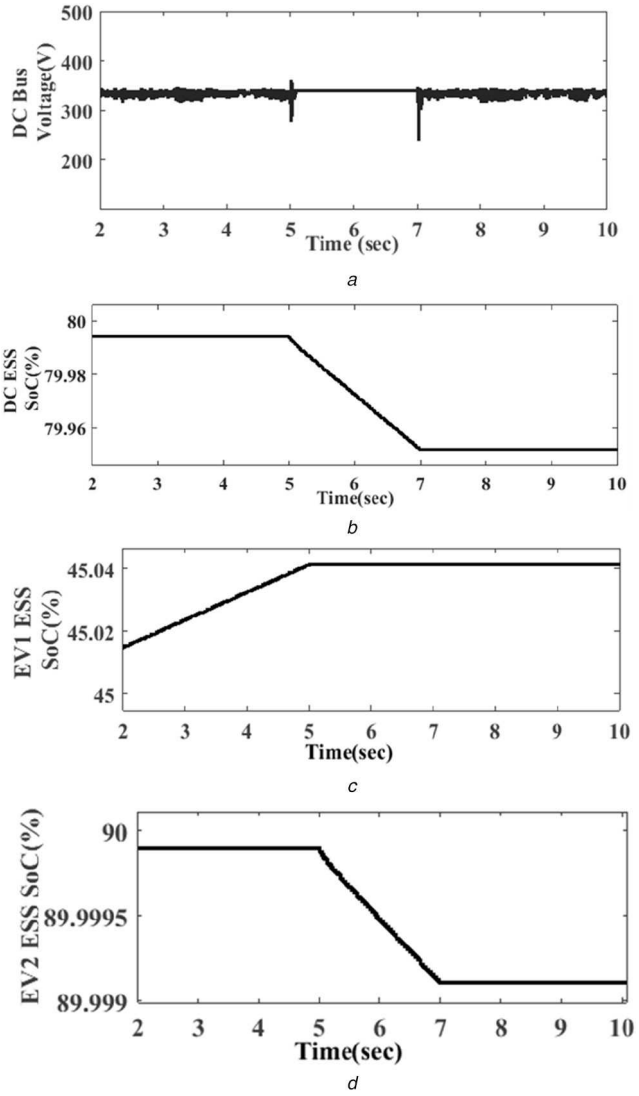

Fig. 12 *System parameters during irradiance variation*
(a) The dc bus voltage, ***(b)*** DC ESS SoC, ***(c)*** EV1 ESS SoC, ***(d)*** EV2 ESS SoC, ***(e)*** Frequency

Table 4 Battery status at different simulation times

	Time	2 s	5 s	7 s
subcase (a) plenty of EV's	EV1 45%	available-charging since SoC<50%	departs-not available	departs-not available
	EV2 90%	not available	arrives-discharging since SoC > 50%	inactive since SoC > 50%
	DC 80%	available, inactive since SoC > 50%	discharges since SoC > 50%	inactive since SoC > 50%

this process, the energy exchanged by DC ESS is 0.46 Wh and EV2 ESS is 0.52 Wh.

Subcase (b) for the condition of minimal EVs is clarified by case I previously and case III in the next session by considering a single EV battery and DC battery. However, in subcase (c) where there are no EVs or the case, which shows non-availability of EV batteries or DC batteries, the system dc voltage drops down and results in system collapse. In this paper, even with 0 EV batteries, DC battery is still considered available in the VPP. This guarantees the safe constant dc voltage for reliability and redundancy of the system since the batteries are connected in parallel. This has been considered as in [47], where the authors have used the main ESS

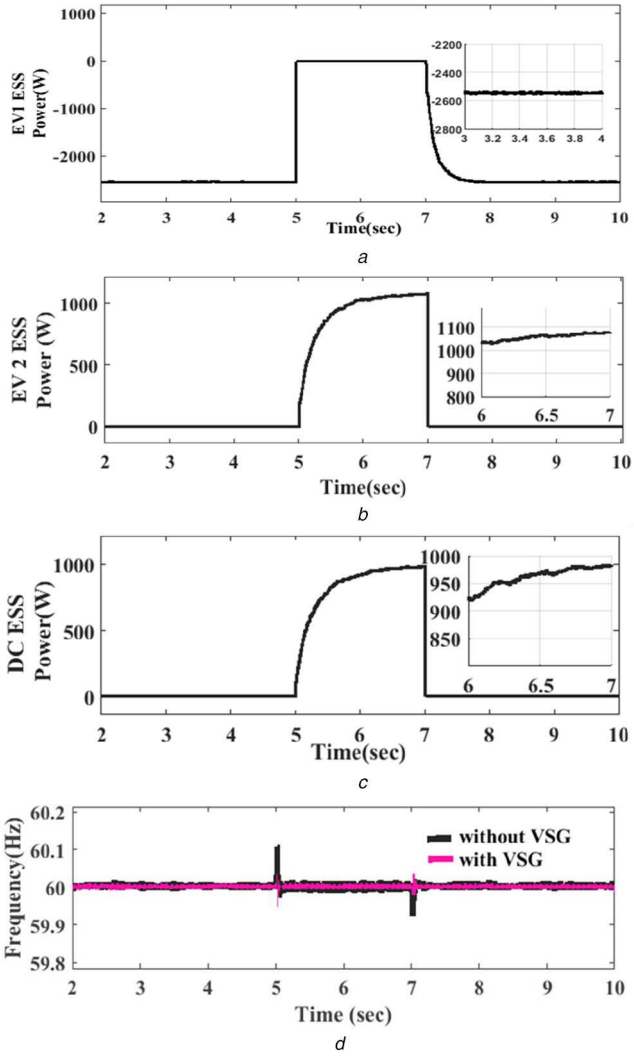

Fig. 13 *Response of ESS's during irradiance variation*
(a) Power exchanged by EV1 ESS, ***(b)*** Power exchanged by EV2 ESS, ***(c)*** Power exchanged by DC ESS, ***(d)*** Frequency

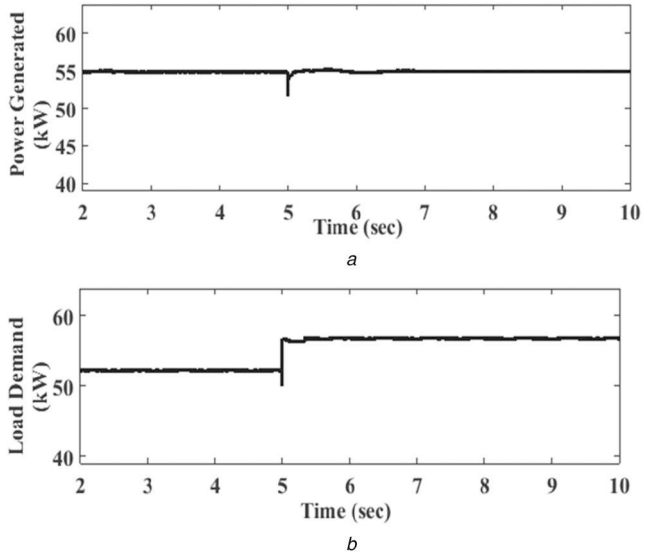

Fig. 14 *Electricity generation & load Profile during load and temperature variation*
(a) Power generated, ***(b)*** Load demand

and sub-ESS for redundancy whenever the circuit is open /there is a fault.

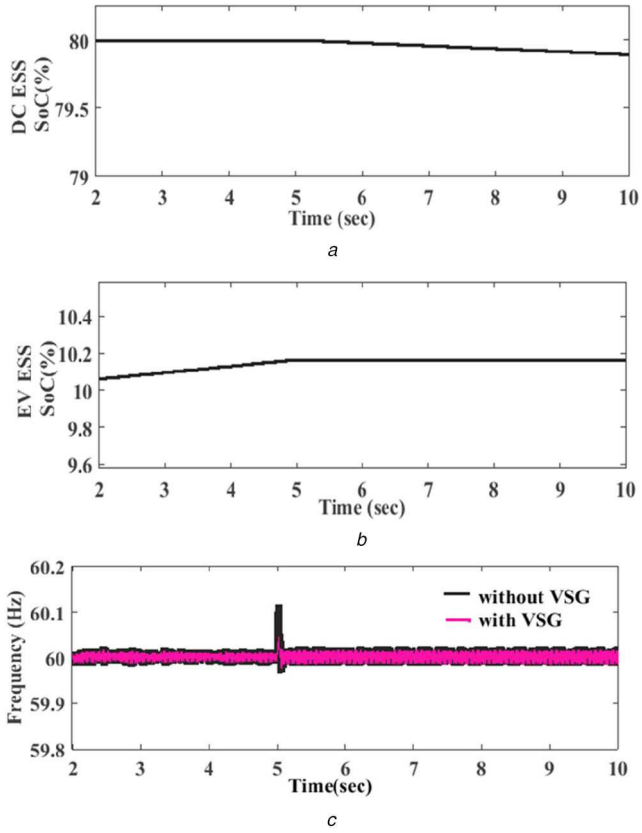

Fig. 15 *System parameters during load and temperature variation*
(a) DC ESS SoC, ***(b)*** EV ESS SoC, ***(c)*** Frequency

4.3 Results and discussion—case study III load and temperature variation

In case study III, the irradiance of the PV system is kept at 1000 W/m^2. The simulations are performed under different conditions of load and temperature. Here the temperature input to the PV array is kept at 50°C and consequently the generation reduced from 25.85 to 23.90 kW as depicted in Fig. 14*a*. Hence the total generation in the system is 54.90 kW. As shown in Fig. 14*b* the load is kept constant at 52.5 kW initially but changed to 56.5 kW after 5 s.

Thus, the change in temperature affects the generation capacity and along with load fluctuations, the system became unstable which leads to frequency fluctuation. Figs. 15*a* and *b* show the SoC status of EV and DC ESS and Fig. 15*c* shows the frequency variations with and without the VSG controller during the load fluctuation. The EV and DC ESS meet the necessary load demand, as the power generation conditions remain constant.

EV ESS charge from the MG until 5 s and absorbs the excess power available since its SoC is <50%. As shown in Fig. 16*a*, the power absorbed by EV ESS until 5 s is −2331 W. The energy exchanged by EV ESS during the charging process is −2.94 Wh. Since the load requirement is increased after 5 s, EV ESS can no longer charge from the MG, and it remains inactive. At the same time, since DC ESS SoC is >50%, it changes from its inactive state to discharging to the MG thereby performing the discharge/grid export mode of operation. DC ESS starts delivering power 1236 W to balance the load demand and generation, shown in Fig. 16*b* and energy exchanged by DC ESS during the discharging process is 1.605 Wh.

EV and DC batteries are added at the dc bus voltage side to reduce the cost of additional supporting devices [48]. The disadvantages of an ac coupled battery system includes limited cost reduction potential, as two full inverters are needed, limited voltage levels of market-available battery inverters for residential applications, which are in the range of 24–48 V, low efficiencies (94%) at the nominal operating point. Here status of only two batteries in cases I and III, and three batteries in case II are shown and this can be used to study the fleet of EVs in a CS and DC batteries that are available in the same geographical area by

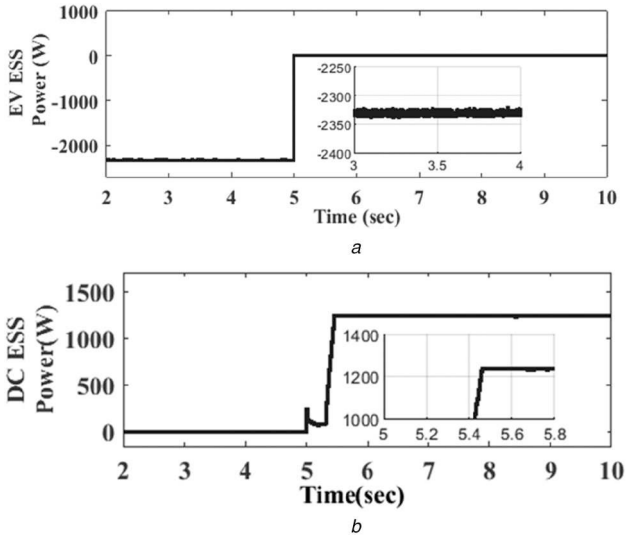

Fig. 16 *Response of ESS's during load and temperature variation*
(a) Power exchanged by EV ESS, ***(b)*** Power exchanged by DC ESS

Table 5 Power flow through VPP components

Power and energy exchanged	Case study I	Case study II	Case study III
power (W)	−2750(EV) 2050(DC)	−2550(EV1) 1050(EV2) 975(DC)	−2331(EV) 1236(DC)
energy (Wh)	−3.53(EV) 2.801(DC)	−3.333(EV1) 0.52(EV2) 0.46 (DC)	−2.94(EV) 1.605(DC)

properly coordinating the bi-directional flow between MG and ESSs. Table 5 details power flow through VPP components in three case studies.

5 Conclusion

This study focuses on the participation of the DCs and EVs to act as a TVPP for providing frequency regulation services using the VI concept. In this research, a battery incorporated system model of VPP represents EVs and DC UPS for emulating inertia for a MG using the VSG concept. VPP effectively monitors the technical operation of charging and discharging in and out of the power system using an EMS. To validate the involvement of different resources and effectiveness of the controller, simulations are performed in MATLAB. It is observed that the frequency variations because of irradiance and load fluctuations are reduced with VPP and VSG controller and it shows better response throughout primary regulation. Charging and discharging operation takes place through a bi-directional dc–dc controller as per the gate signals provided by a VSG powered bi-directional power inverter. The VPP and EMS identify the operation mode and maintains the SoC of the batteries to a safe value by properly islanding the operation if the SoC is not within the pre-set limits. Through this research work based on EV and DC ESS, the authors propose that the ESS from different resources can be used for multiple purposes rather than for a single application. In the future, this analysis can also be extended in the operating cost assessment, which ultimately represents the reduction in battery degradation and extended battery costs during the organisation's expansion period. This work will be a motivation for the investigation of the future expansion of MG with an increased number of RES.

6 References

[1] Dincer, I.: 'Renewable energy and sustainable development: a crucial review', *Renew. Sustain. Energy Rev.*, 2000, **4**, (2), pp. 157–175

[2] I. I. E. Agency.: 'Trends 2018 in photovoltaic applications' (IEA PVPS T1-34), 2018

[3] Kroposki, B., Johnson, B., Zhang, Y.*, et al.*: ' achieving a 100% renewable grid: operating electric power systems with extremely high levels of variable renewable energy', *IEEE Power Energy Mag.*, 2017, **15**, (2), pp. 61–73

[4] Tamrakar, U., Galipeau, D., Tonkoski, R.*, et al.*: 'Improving transient stability of photovoltaic-hydro microgrids using virtual synchronous machines'. 2015 IEEE Eindhoven Powertech Eindhoven, Netherlands, June 29 2015, pp. 1–6

[5] Kabir, M.A., Sajeeb, M.M., Islam, M.N.*, et al.*: 'Frequency transient analysis of countrywide blackout of Bangladesh power system on 1st November, 2014'. 2015 Int. Conf. on Advances in Electrical Engineering (ICAEE), Dhaka Bangladesh, 17 December 2015, pp. 267–270

[6] Haes Alhelou, H., Hamedani-Golshan, M.E., Njenda, T.C.*, et al.*: 'A survey on power system blackout and cascading events: research motivations and challenges', *Energies*, 2019, **12**, (4), p. 682

[7] Dreidy, M., Mokhlis, H., Mekhilef, S.: 'Inertia response and frequency control techniques for renewable energy sources: a review', *Renew. Sustain. Energy Rev.*, 2017, **69**, pp. 144–155

[8] Bevrani, H., Shokoohi, S.: 'An intelligent droop control for simultaneous voltage and frequency regulation in islanded microgrids', *IEEE Trans. Smart Grid*, 2013, **4**, (3), pp. 1505–1513

[9] Sekhar, P.C., Mishra, S.: 'Storage free smart energy management for frequency control in a diesel-PV-fuel cell-based hybrid AC microgrid', *IEEE Trans. Neural Netw. Learn. Syst.*, 2015, **27**, (8), pp. 1657–1671

[10] Zaman, M.S., Wen, Y., Fernandes, R.*, et al.*: 'A cell-level differential power processing IC for concentrating-PV systems with bidirectional hysteretic current-mode control and closed-loop frequency regulation', *IEEE Trans. Power Electron.*, 2015, **30**, (12), pp. 7230–7244

[11] Little, M.L., Rabbi, S.F., Pope, K.*, et al.*: 'Unified probabilistic modeling of wind reserves for demand response and frequency regulation in islanded microgrids', *IEEE Trans. Ind. Appl.*, 2018, **54**, (6), pp. 5671–5681

[12] Parise, G., Martirano, L., Kermani, M.*, et al.*: 'Designing a power control strategy in a microgrid using PID/fuzzy controller based on battery energy storage'. 2017 IEEE Int. Conf. on Environment and Electrical Engineering and 2017 IEEE Industrial and Commercial Power Systems Europe (EEEIC/ I&CPS Europe), Milan Italy, 6 June 2017, pp. 1–5

[13] Beck, H.P., Hesse, R.: 'Virtual synchronous machine'. 2007 9th Int. Conf. on Electrical Power Quality and Utilisation', Barcelona Spain, 9 October 2007, pp. 1–6

[14] Arani, A.K., Gharehpetian, G.B., Abedi, M.: 'Review on energy storage systems control methods in microgrids', *Int. J. Electr. Power Energy Syst.*, 2019, **107**, pp. 745–757

[15] Aly, A.M., Kassem, A.M., Sayed, K.*, et al.*: 'Design of microgrid with flywheel energy storage system using homer software for case study'. 2019 Int. Conf. on Innovative Trends in Computer Engineering (ITCE), Aswan Egypt, 19 February 2019, pp. 485–491

[16] Liu, J., Yang, D., Yao, W.*, et al.*: 'PV-based virtual synchronous generator with variable inertia to enhance power system transient stability utilizing the energy storage system', *Prot. Control Mod. Power Syst.*, 2017, **2**, (1), p. 39

[17] Li, C., Burgos, R., Cvetkovic, I.*, et al.*: 'Evaluation and control design of virtual-synchronous-machine-based STATCOM for grids with high penetration of renewable energy'. 2014 IEEE Energy Conversion Congress and Exposition (ECCE), Pittsburgh, PA, USA, 14 September 2014, pp. 5652–5658

[18] Ma, Y., Cao, W., Yang, L.*, et al.*: 'Virtual synchronous generator control of full converter wind turbines with short-term energy storage', *IEEE Trans. Ind. Electron.*, 2017, **64**, (11), pp. 8821–8831

[19] Liu, J., Miura, Y., Ise, T.: 'Comparison of dynamic characteristics between virtual synchronous generator and droop control in inverter-based distributed generators', *IEEE Trans. Power Electron.*, 2015, **31**, (5), pp. 3600–3611

[20] Wang, R., Chen, L., Zheng, T.*, et al.*: 'VSG-based adaptive droop control for frequency and active power regulation in the MTDC system', *CSEE J. Power Energy Syst.*, 2017, **3**, (3), pp. 260–268

[21] Li, P., Hu, W., Xu, X.*, et al.*: 'A frequency control strategy of electric vehicles in microgrid using virtual synchronous generator control', *Energy*, 2019, **189**, p. 116389

[22] Dhingra, K., Singh, M.: 'Frequency support in a micro-grid using virtual synchronous generator based charging station', *IET Renew. Power Gener.*, 2018, **12**, (9), pp. 1034–1044

[23] Kraftnät, S.: 'Final report Pilot project in demand response and energy storage', Svenska kraftnät, 2018)

[24] Tandukar, P., Bajracharya, L., Hansen, T.M.*, et al.*: 'Real-time operation of a data center as virtual power plant considering battery lifetime'. 2018 Int. Symp. on Power Electronics, Electrical Drives, Automation and Motion (SPEEDAM), Amalfi Italy, 20 June 2018, pp. 81–86

[25] Awasthi, S.R., Chalise, S., Tonkoski, R.: 'Operation of datacenter as virtual power plant'. 2015 IEEE Energy Conversion Congress and Exposition (ECCE), Montreal, QC, Canada, 20 September 2015, pp. 3422–3429

[26] Wang, W., Abdolrashidi, A., Yu, N.*, et al.*: 'Frequency regulation service provision in data center with computational flexibility', *Appl. Energy*, 2019, **251**, p. 113304

[27] Li, S., Brocanelli, M., Zhang, W.*, et al.*: 'Data center power control for frequency regulation'. 2013 IEEE Power & Energy Society General Meeting, Vancouver, BC, Canada, 21 July 2013, pp. 1–5

[28] Tamrakar, U., Shrestha, D., Maharjan, M.*, et al.*: 'Virtual inertia: current trends and future directions', *Appl. Sci.*, 2017, **7**, (7), p. 654

[29] Mohammadi, F., Nazri, G.A., Saif, M.: 'A bidirectional power charging control strategy for plug-in hybrid electric vehicles', *Sustainability*, 2019, **11**, (16), p. 4317

[30] Brocanelli, M., Li, S., Wang, X.*, et al.*: 'Joint management of data centers and electric vehicles for maximized regulation profits'. 2013 int. green computing Conf. Proc., Arlington, VA, USA, 27 June 2013, pp. 1–10

[31] Paananen, J.: 'Data centers as a source of fast frequency response and virtual inertia'. Available at https://www.linkedin.com/pulse/data-centers-source-fast-frequency-response-virtual-inertia-paananen/ (accessed June 2020)
[32] Vandoorn, T.L., Zwaenepoel, B., De Kooning, J.D., *et al.*: 'Smart microgrids and virtual power plants in a hierarchical control structure'. 2011 2nd IEEE PES Int. Conf. and Exhibition on Innovative Smart Grid Technologies, Manchester, UK, 5 December 2011, pp. 1–7
[33] Yavuz, L., Önen, A., Muyeen, S.M., *et al.*: 'Transformation of microgrid to virtual power plant–a comprehensive review', *IET Gener. Transm. Distrib.*, 2019, **13**, (11), pp. 1994–2005
[34] Pourghaderi, N., Fotuhi-Firuzabad, M., Kabirifar, M., *et al.*: 'Energy scheduling of a technical virtual power plant in presence of electric vehicles'. 2017 Iranian Conf. on Electrical Engineering (ICEE), Tehran Iran, 2 May 2017, pp. 1193–1198
[35] Zahedmanesh, A., Muttaqi, K.M., Sutanto, D.: 'A consecutive energy management approach for a VPP comprising commercial loads and electric vehicle parking lots integrated with solar PV units and energy storage systems'. 2019 1st Global Power, Energy and Communication Conf. (GPECOM), Nevsehir, Turkey, Turkey, 12 June 2019, pp. 242–247
[36] Zhou, B., Liu, X., Cao, Y., *et al.*: 'Optimal scheduling of virtual power plant with battery degradation cost', *IET Gener. Transm. Distrib.*, 2016, **10**, (3), pp. 712–725
[37] Thompson, C.C., Oikonomou, P.K., Etemadi, A, *et al.*: 'Optimization of data center battery storage investments for microgrid cost savings, emissions reduction, and reliability enhancement', *IEEE Trans. Ind. Appl.*, 2016, **52**, (3), pp. 2053–2060
[38] Li, S., Bao, K., Fu, X., *et al.*: 'Energy management and control of electric vehicle charging stations', *Electr. Power Compon. Syst.'*, 2014, **42**, (3–4), pp. 339–347
[39] Sayed, K., Gabbar, H.A.: 'Electric vehicle to power grid integration using three-phase three-level AC/DC converter and PI-fuzzy controller', *Energies*, 2016, **9**, (7), p. 532
[40] Shrestha, D., Tamrakar, U., Ni, Z., *et al.*: 'Experimental verification of virtual inertia in diesel generator based microgrids'. 2017 IEEE Int. Conf. on Industrial Technology (ICIT), Toronto, ON, Canada, 22 March 2017, pp. 95–100
[41] Kasera, J., Kumar, V., Joshi, R.R., *et al.*: 'Design of grid connected photovoltaic system employing incremental conductance MPPT algorithm', *J. Electr. Eng.*, 2012, **12**, pp. 172–177
[42] Kumar, N., Hussain, I., Singh, B., *et al.*: 'Peak power detection of PS solar PV panel by using WPSCO', *IET Renew. Power Gener.*, 2017, **11**, (4), pp. 480–489
[43] Agarwal, R., Hussain, I., Singh, B.: 'Three-phase grid-tied single-stage solar energy conversion system using LLMS control algorithm', *IET Renew. Power Gener.*, 2016, **10**, (10), pp. 1638–1646
[44] Seddig, K., Jochem, P., Fichtner, W.: 'Integrating renewable energy sources by electric vehicle fleets under uncertainty', *Energy*, 2017, **141**, pp. 2145–2153
[45] Mohan, V., Singh, J.G., Ongsakul, W., *et al.*: 'Stochastic effects of renewable energy and loads on optimizing microgrid market benefits', *Proc. Technol.*, 2015, **21**, pp. 15–23
[46] Guner, S., Ozdemir, A., Serbes, G.: 'Impact of car arrival/departure patterns on EV parking lot energy storage capacity'. 2016 Int. Conf. on Probabilistic Methods Applied to Power Systems (PMAPS), 16 October 2016, pp. 1–5
[47] Choi, T.S., Ko, J.H., Oh, J.S., *et al.*: 'Operation method of DC micro grid using power control', *J. Int. Counc. Electr. Eng.*, 2019, **9**, (1), pp. 15–23
[48] Vetter, M., Lux, S.: 'Rechargeable batteries with special reference to lithiumion batteries', *Storing Energy*, (Elsevier, 2016), pp. 205–225